Gait & Posture 33 (2011) 645–650

Contents lists available at ScienceDirect

Gait & Posture

journal homepage: www.elsevier.com/locate/gaitpost

Foot bone kinematics as measured in a cadaveric robotic gait simulator

Eric C. Whittaker [a], Patrick M. Aubin [a,b], William R. Ledoux [a,c,d,*]

[a] VA RR&D Center of Excellence for Limb Loss Prevention and Prosthetic Engineering, Seattle, WA, United States
[b] Department of Electrical Engineering, University of Washington, Seattle, WA, United States
[c] Department of Orthopaedics & Sports Medicine, University of Washington, Seattle, WA, United States
[d] Department of Mechanical Engineering, University of Washington, Seattle, WA, United States

ARTICLE INFO

Article history:
Received 2 September 2010
Received in revised form 12 February 2011
Accepted 17 February 2011

Keywords:
Robotics
Gait simulation
Cadaveric simulations
Kinematics
Foot and ankle

ABSTRACT

The bony motion of the foot during the stance phase of gait is useful to further our understanding of joint function, disease etiology, injury prevention and surgical intervention. In this study, we used a 10-segment *in vitro* foot model with anatomical coordinate systems and a robotic gait simulator (RGS) to measure the kinematics of the tibia, talus, calcaneus, cuboid, navicular, medial cuneiform, first metatarsal, hallux, third metatarsal, and fifth metatarsal from six cadaveric feet. The RGS accurately reproduced *in vivo* vertical ground reaction force (5.9% body weight RMS error) and tibia to ground kinematics. The kinematic data from the foot model generally agree with invasive *in vivo* descriptions of bony motion and provides the most realistic description of bony motion currently available for an *in vitro* model. These data help to clarify the function of several joints that are difficult to study *in vivo*; for example, the combined range of motion of the talonavicular, naviculocuneiform, metatarsocuneiform joints provided more sagittal plane mobility (27.4°) than the talotibial joint alone (23.2°). Additionally, the anatomical coordinate systems made it easier to meaningfully determine bone-to-bone motion, describing uniplanar motion as rotation about a single axis rather than about three. The data provided in this study allow for many kinematic interpretations to be made about dynamic foot bone motion, and the methodology presents a means to explore many invasive foot biomechanics questions under near-physiologic conditions.

Published by Elsevier B.V.

1. Introduction

An accurate description of the bony motion of the foot during normal gait can aid in injury prevention, identification of foot abnormalities, surgical correction, and implant design. While *in vivo* foot models with skin-mounted retro-reflective markers are commonly used to describe foot kinematics [1–4], these models suffer from inaccuracies related to skin-motion artifact and rigid body assumptions. Movement of tarsal and midtarsal bones such as the talus, navicular, cuboid, and cuneiforms is often lumped together or ignored since individual bones are very difficult to access; however, these bones have been shown to have significant individual movement in normal feet [5–7]. For example, Nester et al. [5] demonstrated greater motion between the cuneiforms and navicular and between the cuneiforms and cuboid than previously reported in the literature. Making rigid body assumptions within the foot can lead to inaccurate descriptions of the specific joints where motion occurs. Although *in vivo* models using temporary, surgically placed bone pins have provided valuable foot kinematic data [6,7], the highly invasive procedure greatly restricts the use and application of these models with living subjects. Bone pins used in cadaveric models that accurately simulate gait would reduce the need for invasive studies.

In vitro models used with cadaveric feet allow for invasive techniques and access to individual bones of the foot. The main limitation of *in vitro* models is their inability to accurately reproduce physiologic gait. To address this issue, dynamic gait simulators have been used in conjunction with *in vitro* models [5,8,9]. While these simulators are valuable tools in understanding foot bony motion, their accuracy has been affected by the following: non-physiologic ground reaction forces (GRFs) [5], simplified tibial kinematics [5,8,9], low velocity of simulation [8,9], low vertical GRF (vGRF) magnitude [5,8,9], exclusion of bones [9], and technical, rather than anatomical, based coordinate systems [5,8,9]. Our group has developed a cadaveric gait simulator (i.e., the robotic gait simulator or RGS) that has begun to address these issues [10–12], with the intent to provide a more accurate and realistic description of foot kinematics during walking. The aim of this work was to provide a description of the bony motion of the foot during gait and present a methodology (the RGS) that addresses many of the limitations associated with dynamic *in vitro* foot and ankle models of gait.

* Corresponding author at: VA Puget Sound, MS 151, 1660 S. Columbian Way, Seattle, WA 98108, United States. Tel.: +1 206 768 5347; fax: +1 206 277 3963.
E-mail address: wrledoux@u.washington.edu (W.R. Ledoux).

0966-6362/$ – see front matter. Published by Elsevier B.V.
doi:10.1016/j.gaitpost.2011.02.011

Table 1
A 10-segment kinematic foot model with anatomical coordinate systems. Not shown in foot model diagram are the four quad marker clusters in the TAL, NAV, CUN, and CUB.

Markers

Real markers
(1) Proximal tibia shaft
(2) Distal tibia shaft
(3) Lateral malleolus
(4) Medial malleolus
(5) Inferior portion of posterior aspect of calcaneus
(6) Superior portion of posterior aspect of calcaneus
(7) Most medial point on sustentaculum tali
(8) Most lateral point on trochlear process
(9–12) 4-marker rod extending from the talus
(13–16) 4-marker rod extending from the navicular
(17–20) 4-marker rod extending from the medial cuneiform
(21–24) 4-marker rod extending from the cuboid
(25) Base of the first metatarsal
(26) Superior to #25 on 2-marker rod on base of first metatarsal
(27) Head of the first metatarsal
(28) Superior to #27 on 2-marker rod on head of first metatarsal
(29–32) Same pattern as #25–28, except on third metatarsal
(33–36) Same pattern as #25–28, except on fifth metatarsal
(37–40) Same pattern as #25–28, except on proximal phalanx

Segment definitions for a left foot
TIB (tibia and fibula): primary = #2 → #1, dummy = #4 → #3, order = *yxz*
TAL (talus): primary = #v3 → #v1, dummy = #v3 → #v2, order = *xyz*
CALC (calcaneus): primary = #5 → #6, dummy = #7 → #8, order = *yxz*
NAV (navicular): primary = #v6 → #v4, dummy = #v4 → #v5, order = *zxy*
CUN (medial cuneiform): primary = #v9 → #v7, dummy = #v7 → #v8, order = *zxy*
CUB (cuboid): primary = #v10 → #12, dummy = #v11 → #12, order = *xyz*
MET1 (first metatarsal): primary = #25 → #27, dummy = #26 → #25, order = *xzy*
MET3 (third metatarsal): primary = #29 → #31, dummy = #32 → #31, order = *xzy*
MET5 (fifth metatarsal): primary = #33 → #35, dummy = #36 → #35, order = *xzy*
HAL (proximal phalanx): primary = #37 → #39, dummy = #40 → #39, order = *xzy*

Virtual/digitized points
(v1) Most lateral point of talar head
(v2) Most medial point of talar head
(v3) Trigonal process
(v4) Tuberosity of navicular
(v5) Most superior point on dorsal surface of navicular, half way between distal and proximal edges
(v6) Lateral border of dorsal surface of navicular
(v7) Most medial point on medial surface of medial cuneiform
(v8) Most superior point on dorsal surface of intermediate cuneiform, half way between distal and proximal edges
(v9) Most lateral point on dorsal surface of lateral cuneiform
(v10) Most posterior, medial point on dorsal surface of cuboid
(v11) Most anterior, lateral point on dorsal surface of cuboid
(v12) Most anterior, medial point on dorsal surface of cuboid

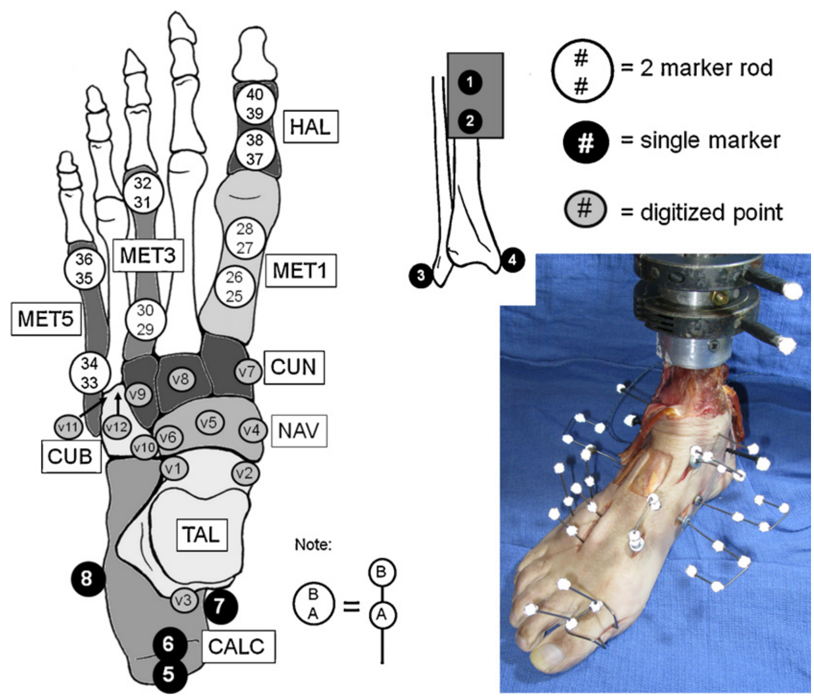

2. Methods

For this IRB-approved study, six fresh-frozen cadaveric lower limb specimens (age: 75.8 ± 6.1 yrs, 5 male, 1 female, two pairs, two unpaired) with neutral bony alignment, transected approximately 12 cm proximal to the ankle joint, were identified by an orthopedic surgeon using X-rays. Approximately 10 cm of each of nine extrinsic ankle tendons were dissected and attached to aluminum or plastic tendon clamps. After applying the foot model marker set described below, the cadaveric specimen was mounted into the RGS using a custom tibia mounting device.

The RGS consists of an R2000 six-degree of freedom (DOF) parallel robot (Mikrolar Inc., Hampton, NH), nine brushless DC linear tendon force actuators (Exlar Corp., Chanhassen, MN) in series with nine load cells (Transducer Techniques Inc., Temecula, CA), a force plate (Kistler Instrument Corp., Amherst, NY), a real time PXI embedded controller (National Instruments Corp., Austin, TX), a six-camera motion analysis system (Vicon, Lake Forest, CA), and a PC user interface, all synchronized to a 5 V trigger at heel strike. The motion of the RGS is prescribed from kinematic data of living subjects. Target tibial kinematics and GRFs were recorded from 10 subjects performing four or five repeated gait trials in our motion analysis lab. A 12-camera motion analysis system (Vicon, Lake Forest, CA) sampling at 120 Hz or 250 Hz recorded the motion of the tibial coordinate system (TIB), while a force plate (Bertec Corporation, Columbus, OH) sampling at 600 Hz or 1500 Hz recorded the GRF. The RGS also requires target muscles forces, which were estimated from literature [13–17] using an EMG to force model with a 42 ms electromechanical delay [18].

To simulate gait, the tibia was held fixed while the R2000 moved the mobile force plate according to the target *in vivo* tibial kinematics to recreate the relative tibia to ground motion. Tendon force was controlled by a real time nine-axis PID force controller running on the PXI. The *in vitro* vGRF was controlled with a fuzzy logic controller which altered the target tibialis anterior tendon force (real time), Achilles tendon force (real time), and tibial kinematics (iteratively) to accurately track the target *in vivo* vGRF. For each foot, three simulation quartets were collected, each containing three learning trials and one final trial. The learning trials allowed the vGRF fuzzy logic controller to slightly adjust the position of the force plate normal to the foot, and also allowed preconditioning of the plantar surface soft tissue, providing more repeatable GRF data. During the fourth trial of all quartets, the bony motion of the cadaveric foot was recorded with the six-camera motion analysis system.

A 10-segment, 40-marker *in vitro* kinematic foot model with anatomical coordinate systems was constructed with 6.4 mm retro-reflective markers. In general, the coordinate systems were aligned to the cardinal planes, and do not necessarily reflect the axes of rotation of the individual bones, especially for the smaller bones such as the cuneiforms and cuboid. The TIB, calcaneus (CALC), first metatarsal (MET1), third metatarsal (MET3), fifth metatarsal (MET5), and hallux (HAL) anatomical coordinate systems were created from retro-reflective markers attached to each bone at specific locations with bone pins (Table 1). Quad marker clusters in an arbitrary orientation were attached to the talus (TAL), navicular (NAV), cuboid (CUB), and medial cuneiform (CUN) with screws. For these four bones, a stylus wand with four markers was used during a static calibration

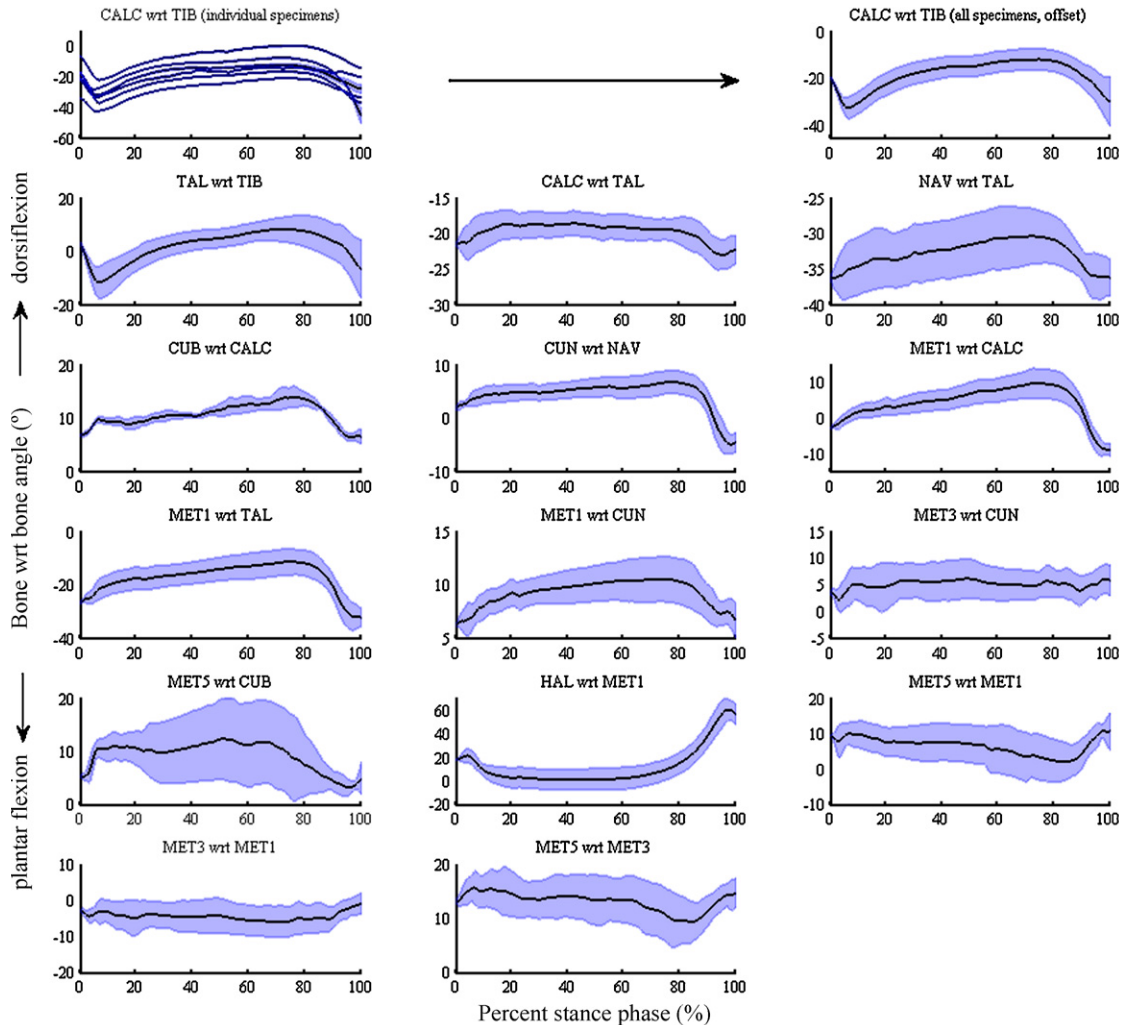

Fig. 1. The mean ± 1 SD bone with respect to (wrt) bone angular motion in the sagittal plane; CALC wrt TIB plots demonstrate conversion from 6 individual specimen averages to the offset all-specimen average; note: *y*-axes were individually scaled to fit data ranges and show trends; more positive values are dorsiflexion, more negative values are plantar flexion.

procedure to create virtual markers by referencing the locations of three anatomical landmarks per bone with respect to that bone's quad cluster coordinate system. For the CUN segment, a quad was placed in the medial cuneiform to track motion, while virtual points from all three cuneiforms were used to generate the anatomical coordinate system. Anatomical coordinate systems for the talus, navicular, cuboid, and medial cuneiform bones were then created from the virtual markers. For each segment, a primary axis was defined by two markers. A dummy axis crossed with the primary axis defined the secondary axis. The third axis was defined by the right hand rule and the order token (e.g., order = *yxz*) which defined the name of the first (*y*), second (*x*) and third axes (*z*) (Table 1). In general, the positive *x*-axis pointed anteriorly, the positive *y*-axis pointed superiorly, and the positive *z*-axis pointed medially for left feet and laterally for right feet.

During the *in vitro* dynamic gait simulation, the six-camera motion analysis system recorded the position of the 40 markers at 200 Hz. A custom Body Builder (Vicon, Lake Forest, CA) program determined the motion of the virtual points from the quad marker clusters and calculated the anatomical *zxy* fixed angle descriptions for 10 joints and six bone-to-bone relationships. The kinematic data were filtered with a 10 Hz zero phase low pass Butterworth filter. To examine the unique bony motion of each specimen, range of motion (ROM) for each bone-to-bone relationship was calculated and the mean and standard deviations (SDs) were determined. For time-series visualization purposes (Figs. 1–3), inter-specimen angular data were shifted to the mean value (averaged across all 18 trails) at heel strike. The mean ± 1 SD values for all 18 trials were plotted after this offset was applied, allowing for a succinct representation and alignment of the rotational trends while still accounting for specimen repeatability and variability.

3. Results

The fuzzy logic vGRF controller demonstrated its ability to track the target vGRF with high fidelity for six cadaveric specimens [12]. The average RMS error between the target *in vivo* and actual *in vitro* vGRF was 5.9% body weight (BW) across all 18 final trials. The RGS was able to replicate the *in vivo* kinematics of TIB with respect to GND. All three fixed angles of the tibia with respect to the ground were almost entirely within ±1 SD of those found *in vivo* for all feet except for the sagittal plane angle, which was within 0.5° of ±1 SD from approximately 75 to 95% of stance phase. Average root mean squared (RMS) tracking error for all tendons except for the fuzzy logic-controlled tibialis anterior and Achilles was 3.9 N for all trials.

The mean ± 1 SD total ROM was calculated for all 17 kinematic relationships, i.e., joints (Table 2). In general, inter-trial joint motion was repeatable (Figs. 1–3, top left plot). Intra-specimen SDs were often less than ±1°, and rarely exceeded ±2°. The mean ± 1 SD kinematic patterns for joints of particular interest were determined for the sagittal, coronal, and transverse planes (Fig. 1, Fig. 2, and Fig. 3, respectively). Cuboid digitization errors and quad cluster movement after digitization required removing cuboid data from 11 trials resulting in only 7 trials from a total of 3 feet for motions involving the cuboid.

In the sagittal plane, the talotibial joint (TAL wrt TIB) and calcaneotibial complex (CALC wrt TIB) had similar behavior; plantar flexion at heel strike was followed by dorsiflexion during midstance and plantar flexion during push off (Fig. 1). The total ROM in the sagittal plane for the talotibial joint and calcaneotibial complex was 23.2° and 23.6°, respectively (Table 2). The first metatarsal with respect to the talus (MET1 wrt TAL) and calcaneus

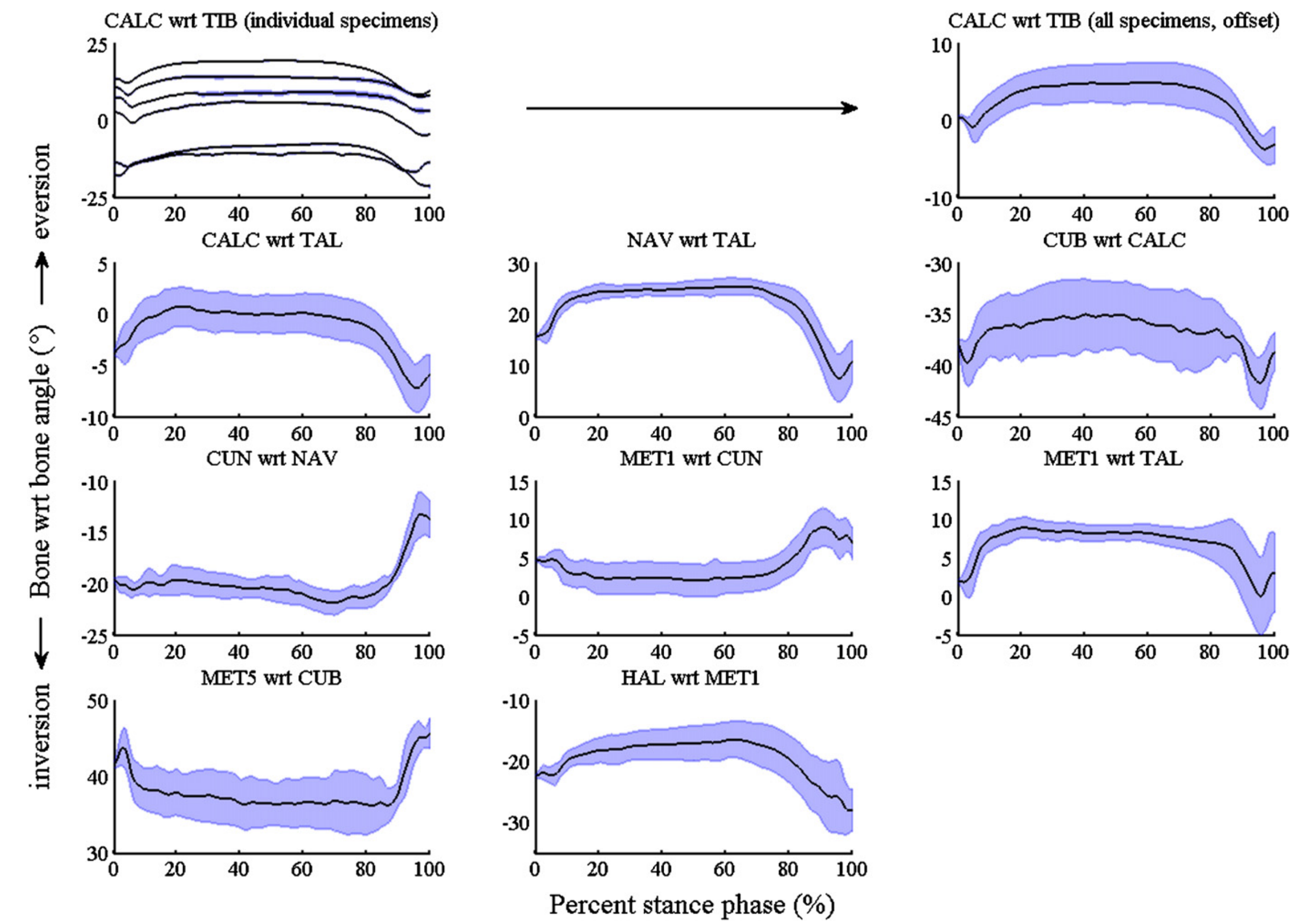

Fig. 2. The mean ± 1 SD bone with respect to (wrt) bone angular motion in the coronal plane; CALC wrt TIB plots demonstrate conversion from 6 individual specimen averages to the offset all-specimen average; note: *y*-axes were individually scaled to fit data ranges and show trends; more positive values are eversion, more negative values are inversion.

(MET1 wrt CALC) and the talonavicular (NAV wrt TAL), calcaneocuboid (CUB wrt CALC), naviculocuneiform (CUN wrt NAV) and first metatarsocuneiform (MET1 wrt CUN) joints all dorsiflexed from heel strike until approximately 75% of stance phase at which time they plantar flexed (Fig. 1). The subtalar joint (CALC wrt TAL) showed minimal motion throughout stance phase (6.8° total ROM) (Table 2 and Fig. 1). The cuboid-fifth metatarsal joint (MET5 wrt CUB) had a greater total ROM (12.3°) than the third metatarsal with respect to the medial cuneiform (MET3 wrt CUN) (7.4°) (Table 2). At the forefoot, the fifth metatarsal in relation to the third showed

Table 2
Mean ± 1 SD ROM for all 18 trials. Data in (parentheses) are from Lundgren et al. [6]. Bold and underlined values are within ±1 SD of the data reported by Lundgren et al. Underlined values are within ±2 SD of the data reported by Lundgren et al. Cuboid digitization errors and quad cluster movement after digitization required 11 trials to be discarded during post processing.

Child bone wrt parent bone angle (°)	Number of specimens, trials included	Sagittal plane average ROM ± 1 SD	Coronal plane average ROM ± 1 SD	Transverse plane average ROM ± 1 SD
TIB wrt GND	6, 18	59.2 ± 1.0	26.1 ± 2.2	10.4 ± 2.5
TAL wrt TIB	6, 18	23.2 ± 4.6 (15.3 ± 2.0)	**6.2 ± 3.8** (8.1 ± 3.8)	11.0 ± 6.5 (7.8 ± 2.7)
CALC wrt TAL	6, 18	**6.8 ± 1.9** (6.8 ± 1.4)	**8.6 ± 2.5** (9.8 ± 1.8)	**6.2 ± 2.3** (7.5 ± 2.0)
CALC wrt TIB	6, 18	23.6 ± 7.0 (17.0 ± 2.1)	**9.2 ± 3.0** (11.3 ± 3.5)	10.7 ± 3.6 (7.3 ± 2.4)
NAV wrt TAL	6, 18	9.6 ± 4.6 (8.4 ± 1.1)	**18.8 ± 4.8** (14.9 ± 6.1)	**14.9 ± 5.5** (16.3 ± 6.5)
CUB wrt CALC	3, 7	**8.8 ± 1.9** (9.7 ± 5.2)	**8.6 ± 0.5** (11.3 ± 3.9)	**7.5 ± 1.8** (8.1 ± 2.0)
CUN wrt NAV	6, 18	**12.2 ± 2.2** (11.5 ± 1.8)	**9.4 ± 2.4** (10.4 ± 6.3)	**5.8 ± 2.8** (6.2 ± 4.2)
CUB wrt NAV	3, 7	18.7 ± 9.4 (7.2 ± 2.4)	**4.9 ± 3.0** (8.8 ± 4.4)	20.1 ± 11.1 (8.9 ± 4.3)
MET1 wrt CALC	6, 18	19.9 ± 5.1	8.0 ± 3.6	11.9 ± 3.0
MET1 wrt TAL	6, 18	22.6 ± 6.4 (17.6 ± 2.7)	**11.4 ± 4.1** (9.6 ± 4.2)	**19.5 ± 3.8** (14.7 ± 5.3)
MET1 wrt CUN	6, 18	**5.6 ± 2.3** (5.3 ± 2.0)	8.5 ± 2.5 (5.4 ± 1.0)	**5.5 ± 2.1** (6.1 ± 1.1)
MET3 wrt CUN	6, 18	7.4 ± 1.5	5.8 ± 2.2	7.0 ± 2.4
MET5 wrt CUB	3, 7	**12.3 ± 5.7** (13.3 ± 1.4)	**11.9 ± 1.3** (10.4 ± 3.7)	**9.1 ± 5.9** (9.8 ± 2.1)
HAL wrt MET1	6, 18	61.9 ± 7.0	13.2 ± 3.9	18.4 ± 7.5
MET5 wrt MET1	6, 18	12.5 ± 4.5	12.0 ± 3.4	8.8 ± 6.6
MET5 wrt MET3	6, 18	9.8 ± 3.2	7.0 ± 1.9	8.4 ± 5.1
MET3 wrt MET1	6, 18	8.2 ± 3.0	9.5 ± 3.4	7.3 ± 2.2

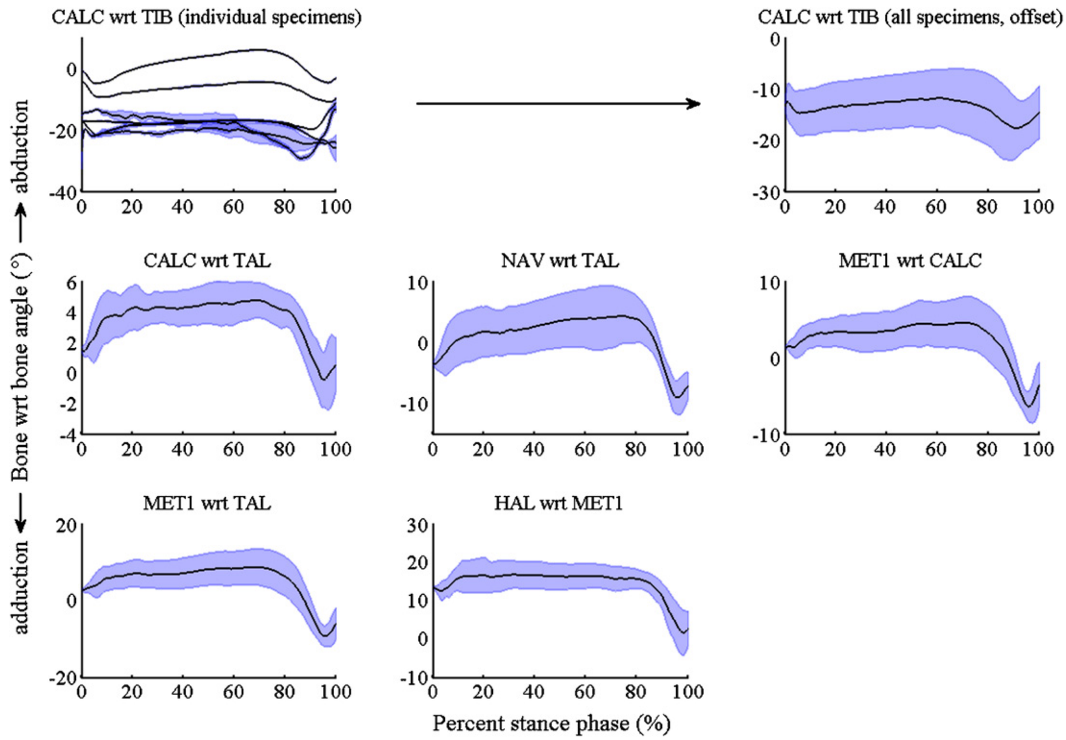

Fig. 3. The mean ± 1 SD bone with respect to (wrt) bone angular motion in the transverse plane; CALC wrt TIB plots demonstrate conversion from 6 individual specimen averages to the offset all-specimen average; note: *y*-axes were individually scaled to fit data ranges and show trends; more positive values are abduction, more negative values are adduction.

slightly more movement (9.8°) than the third in relation to the first (8.2°) (Table 2). The first metatarsophalangeal joint (HAL wrt MET1) plantar flexed at heel strike, remained constant throughout foot flat, and dorsiflexed during push off (61.9° of total ROM) (Table 2 and Fig. 1).

In the coronal plane, the first metatarsal with respect to the talus, and the subtalar, talonavicular, and calcaneocuboid joints everted during the loading response, remained relatively constant throughout foot flat, and then inverted during push off (11.4°, 8.6°, 18.8°, and 8.6° of total ROM, respectively) (Table 2 and Fig. 2). The naviculocuneiform, metatarsocuneiform, and cuboid-fifth metatarsal joints were relatively constant during heel strike and midstance but everted during late stance (9.4°, 8.5°, and 11.9° of total ROM, respectively) (Table 2 and Fig. 2). The first metatarsophalangeal joint slightly everted throughout midstance and then inverted during late stance (13.2° of total ROM) (Table 2 and Fig. 2).

In the transverse plane, the first metatarsal with respect to the calcaneus, first metatarsal with respect to the talus, the subtalar, the talonavicular, and the first metatarsophalangeal joints all slightly abducted at heel strike, remained relatively constant throughout foot flat, and then adducted during push off (11.9°, 19.5°, 6.2°, 14.9° and 18.4° of total ROM, respectively) (Table 2 and Fig. 3).

4. Discussion

Quantifying the bony motion of the foot and ankle during gait has the potential to advance our understanding of its normal and pathologic function and assist clinical decision making. In general, we found good agreement between our kinematic data and data from *in vivo* studies, especially Lundgren et al.'s study employing bone pins [6], which will be considered the gold standard for *in vivo* bony motion during gait. The total ROM reported here was within ±1 SD of the data reported by Lundgren et al. for 21 out of 30 angular measurements, while 25 of the 30 reported angles were within ±2 SD of the data reported by Lundgren et al. Many commonly observed kinematic characteristics of gait were reproduced with the gait simulator. For example, our results were supported by the following findings from *in vitro* and *in vivo* studies: tri-planar motion of the subtalar joint [6,19]; calcaneus to tibia motion of plantar flexion and eversion (loading response), followed by dorsiflexion (midstance), then plantar flexion and inversion (push off) [5,6]; independent motion of the first and fifth rays [5,8]; considerable tri-planar motion of the first and fifth metatarsals, especially when used as arch height descriptors in relation to proximal bones [6]; and greater tri-planar motion in the talonavicular joint (especially in coronal and transverse planes) than that of the subtalar joint [6]. One minor unexpected result we observed was a brief moment of inversion of the calcaneotibial complex from approximately 0 to 3% of stance phase. Due to the effect of gravity and static tendon forces on the calcaneus in its pre-impact position, it is possible that this brief inversion is a non-physiologic, methodological artifact.

There were several other interesting results from our work, most of which provide additional support to studies that describe considerable motion at joints (especially in the midfoot) where it might not be expected. Studies that model the midfoot as a rigid body assume that the talotibial joint contributes to most of the foot's mobility in the sagittal plane. We found, however, that the combined ROM of the talonavicular (9.6°), naviculocuneiform (12.2°), and metatarsocuneiform (5.6°) joints provided substantial sagittal plane mobility in relation to the talotibial joint alone (23.2°) (Table 2). These data confirm that the midfoot is an important contributor to sagittal plane motion. The amount of motion in the midfoot also highlights the importance of other midfoot joints besides the midtarsal joint, which is often emphasized in the literature [20]. As stated above, the naviculocuneiform joint, which is commonly thought to have little motion, showed more sagittal plane ROM than the talonavicular joint. Important motion outside the midtarsal joint was further supported in the lateral foot, where the cuboid-fifth metatarsal joint had greater sagittal plane total ROM (12.3°) than the calcaneocuboid joint (8.8°). Thus, in our study, the midtarsal joint provided less than half of the forefoot's sagittal plane mobility, both medially and laterally. Of course, this finding does not detract from the relevance of the midtarsal joint; it did have substantial motion in the coronal and transverse planes (Table 2). While the talonavicular and calcaneocuboid joints shared a common pattern of dorsiflexion followed by plantar flexion, we found more motion (as determined from only 7 trials for 3 feet) between the navicular and cuboid (18.7° sagittal, 4.9° coronal, 20.1° transverse) than at the calcaneocuboid joint (8.8° sagittal, 8.6° coronal, 7.5° transverse). Thus, as supported by Lundgren et al. [6], the navicular and cuboid bones are best not modeled as a rigid body.

The chosen coordinate systems allowed for an anatomical description of the position and orientation of the distal bone relative to the proximal bone in the cardinal planes. The anatomical bone-to-bone orientation is an important measurement when investigating pathologies that affect initial bony alignment such as pes planus and pes cavus foot deformities, as it is easier to meaningfully explain bone-to-bone motion. For example, uniplanar motion such as calcaneal eversion can be described as rotation in a single plane (frontal) rather than in three planes, as would be the case if the coordinate system was arbitrary.

There were potential limitations in our study. The precision of anatomical coordinate systems in the foot has been shown to decrease for smaller foot segments [21], as angular accuracy and precision of a vector defined by two points is inversely proportional to the distance between the two points. Thus, in general, we digitized points as far apart on a bone as reasonably possible for all bones except the medial cuneiform. Due to this bone's small size, we digitized points on the intermediate and lateral cuneiforms as well. Intermediate and lateral cuneiform motion was not recorded in this study, therefore MET3 wrt CUN refers to the third metatarsal relative to the medial cuneiform, which is a limitation when describing motion in the kinematic chain. For all digitized bones, unavoidable inter-specimen variability was created by the digitization of small anatomical landmarks that can be difficult to find accurately and precisely on different feet. Next, we did not normalize the tibial kinematic input data to the RGS by foot size. Kinematics at push off can be different for a longer foot than a shorter foot, as the hallux remains on the force plate for a greater amount of time and is taken through a larger ROM. This effect may be evident in our study, as the average ROM of the first metatarsophalangeal joint was 61.9° compared to 42° as determined by Nawoczenski et al. [22]. The *in vivo* variability inherent to the tibial kinematic inputs was also not accounted for during the *in vitro* simulations, which may have artificially decreased variability in distal joints of the foot. Lastly, our cadaveric model did not simulate the intrinsic musculature force of the foot.

This study provided a description of foot bone motion using a biomechanically realistic gait simulator (the RGS) and by incorporating anatomical coordinate systems. Our kinematic data generally agree with invasive *in vivo* descriptions of bony motion and provides the most realistic description of bony motion currently available for an *in vitro* model. The large sagittal plane motion, provided by joints other than the ankle, demonstrates the significant limitations of historical models of the foot. The kinematic data helps to clarify and/or support recent descriptions of the function of several joints that are difficult to study *in vivo*, providing confidence in the current understanding of foot bone motion. Our methodology presents a means to explore many invasive foot biomechanics questions under near-physiologic conditions.

Acknowledgements

This work was funded in part by the Department of Veterans Affairs Rehabilitation Research and Development Service grants A3923R and A6669R.

Conflict of interest statement

The authors have no conflicts to report.

References

[1] Khazzam M, Long JT, Marks RM, Harris GF. Preoperative gait characterization of patients with ankle arthrosis. Gait Posture 2006;24:85–93.
[2] Jenkyn T, Anas K, Nichol A. Foot segment kinematics during normal walking using a multisegment model of the foot and ankle complex. J Biomech Eng 2009;131:034504.
[3] Leardini A, Benedetti M, Berti L, Bettinelli D, Nativo R, Giannini S. Rear-foot, mid-foot and fore-foot motion during the stance phase of gait. Gait Posture 2007;25:453–62.
[4] Simon J, Doederlein L, McIntosh A, Metaxiotis D, Bock H, Wolf S. The Heidelberg foot measurement method: development, description and assessment. Gait Posture 2006;23:411–24.
[5] Nester CJ, Liu AM, Ward E, Howard D, Cocheba J, Derrick T, et al. In vitro study of foot kinematics using a dynamic walking cadaver model. J Biomech 2007;40:1927–37.
[6] Lundgren P, Nester CJ, Liu A, Arndt A, Jones R, Stacoff A, et al. Invasive in vivo measurement of rear-, mid- and forefoot motion during walking. Gait Posture 2008;28:93–100.
[7] Arndt A, Wolf P, Liu A, Nester C, Stacoff A, Jones R, et al. Intrinsic foot kinematics measured in vivo during the stance phase of slow running. J Biomech 2007;40:2672–8.
[8] Okita N, Meyers S, Challis J, Sharkey N. An objective evaluation of a segmented foot model. Gait Posture 2009;30:27–34.
[9] Hurschler C, Emmerich J, Wulker N. In vitro simulation of stance phase gait – part I: model verification. Foot Ankle Int 2003;24:614–22.
[10] Aubin P, Cowley M, Ledoux W. Gait simulation via a 6-DOF parallel robot with iterative learning control. IEEE Trans Biomed Eng 2008;55:1237–40.
[11] Bayomy AF, Aubin PM, Sangeorzan BJ, Ledoux WR. Arthrodesis of the first metatarsophalangeal joint: a robotic cadaveric study of dorsiflexion angle. J Bone Joint Surg Am 2010;92:1754–64.
[12] Aubin, Patrick M. The Robotic Gait Simulator: A Dynamic Cadaveric Foot and Ankle Model for Biomechanics Research, PhD Dissertation. Department of Electrical Engineering, Universitynof Washington.
[13] Ishikawa M, Komi P, Grey M, Lepola V, Bruggemann G. Muscle–tendon interaction and elastic energy usage in human walking. J Appl Physiol 2005;99:603–8.
[14] Wickiewicz T, Roy R, Powell P, Edgerton V. Muscle architecture of the human lower-limb. Clin Orthop Relat Res 1983;275–83.
[15] Pierrynowski MR. A physiological model for the solution of individual muscle forces during normal human walking. Simon Fraser University; 1982.
[16] Fukunaga T, Roy R, Shellock F, Hodgson J, Edgerton V. Specific tension of human plantar flexors and dorsiflexors. J Appl Physiol 1996;80:158–65.
[17] Perry J. Gait analysis: normal and pathological function. Thorofare, NJ: SLACK Incorporated; 1992.
[18] Zhou S, Lawson D, Morrison W, Fairweather I. Electromechanical delay in isometric muscle contractions evoked by voluntary, reflex and electrical-stimulation. Eur J Appl Physiol 1995;70:138–45.
[19] Wong Y, Kim W, Ying N. Passive motion characteristics of the talocrural and the subtalar joint by dual Euler angles. J Biomech 2005;38:2480–5.
[20] Blackwood CB, Yuen TJ, Sangeorzan BJ, Ledoux WR. The midtarsal joint locking mechanism. Foot Ankle Int 2005;26:1074–80.
[21] Brown KM, Bursey DE, Arneson LJ, Andrews CA, Ludewig PM, Glasoe WM. Consideration of digitization precision when building local coordinate axes for a foot model. J Biomech 2009;42:1263–9.
[22] Nawoczenski D, Baumhauer J, Umberger B. Relationship between clinical measurements and motion of the first metatarsophalangeal joint during gait. J Bone Joint Surg Am 1999;81A:370–6.